Clinical Cancer Investigation Journal-ISSN: 2278-0513

# Studying the Optical and Electrical Properties of aluminum (Al)-Coated Zinc Oxide Thin Films


## Abstract

The present study aims to investigate the optical and electrical characteristics of aluminum (Al)-coated zinc oxide thin films. The samples in this section were prepared with Sol-Gel method.Using Puma software, the film thickness is around 200 nm. The X-ray diffraction spectrum of these samples comprises three peaks owing to diffraction from plates (100), (002), and (101) associated with the creation of a hexagonal structure of zinc oxide, according to the results of characterization. Sample contamination reduces peak intensity (002) substantially. The resistivity of the synthesized films falls by a little quantity of impurity to a significant order, such that the sample's specific strength has a minimum impurity of roughly 2% and increases again with the addition of further impurities, according to these tests. With a minimal impurity of roughly 2%, the sample's specific strength increases and then decreases when more impurities are added. Furthermore, the adsorption edge of impurity-free samples is in the 370 nm wavelength region, which moves to lower energies as the number of impurities rises.


**Keywords:** *Zinc oxide nanoparticles, transparent conductive thin films, aluminum*


**[1]Zahra Ameri**

*1 Department of engineering , University of Applied Science and Technology, Shahroud, Semnan, Iran.*

*Z.ameri65@gmail.com*


## 1. Introduction

Miniaturization of optoelectronic components and nanotechnology have become more important as technology has advanced in recent years. Nanotechnology is defined by the scale of 0.1 to 100 nanometers. Because of the increased surface-to-volume ratio, materials with dimensions in this range can exhibit novel characteristics [1]. The world is transforming thanks to nanotechnology. Today, there are hundreds of firms working in the field of nanotechnology. Nanotechnology research and development cost more than $ 3 billion worldwide in 2003 [1]. Nanomaterials exports are expected to increase from $ 125 million at the end of the twentieth century to $ 35 billion by the end of the twenty-first century [1]. Given nanotechnology's interdisciplinary impact in various scientific and industrial fields, as well as its numerous applications in fields such as electronics and computers, communications, medicine, and medicine, it can be claimed that this technology has caused the convergence of various scientific disciplines and that the start of activities in it can cause leaps in various fields.

Semiconductor contamination is one of the most critical concerns in semiconductor physics. The electrical characteristics of a semiconductor will be significantly affected by the presence of small and controlled concentrations of particular impurities (contamination) [2]. When semiconductors are polluted, their electrical and optical characteristics are frequently altered compared to non-contaminated samples. The semiconductor optical band gap is one of these factors, which is frequently related to Moss-Burstein shift [3] or Many-body effects [4]. When free electrons are introduced to the structure of semiconductor materials, they occupy the conduction edge. As a result, electrons stimulated from the capacitance band to the conduction band need more energy, increasing the material's bandgap. The Moss-Burstein shift is the change in the size of the bandgap.

Thin films, on the other hand, are among the structures that have changed the most as a result of nanotechnology. The study and investigation of surface physics, common ground, and solid surfaces blossomed from the early 1960s onwards, leading to significant discoveries in nanotechnology [5]. Today, thin coatings of transparent conductive oxides are used in a variety of sectors, including microelectronics, optoelectronics, and aerospace [6]. Additionally, many electrical and optoelectronic components, such as gas sensors, solar cells, and screens, are made with them. Clear conductive oxides are exceptional compounds with unique physical features such as great optical clarity in the visible range (about 75 to 90%) and high electrical conductivity (around $10^{-2}$ Ωcm) [7]. Zinc oxide (ZnO) is a widely used transparent conductive oxide that belongs to the IV-II semiconductor family and has a straight and broad bandgap (eV3 / 3), good transparency, rapid electron mobility, and significant excitonic energy (meV60) [8]. Zinc oxide has a wide range of uses in the optoelectronic industry, including displays, light-emitting diodes, transistors, heat protection windows, solar cells, and gas sensors [9-10] due to its unique features. Many groups have predicted the band structure of zinc oxide [11]. Fan et al. provided an example of this type of study. Using the EPM (Empirical Pseudopotential method) approach. Numerous experimental reports of bandgap size determined using experimental data such as trajectory spectra have been

published in major scientific publications [13-12], in addition to theoretical calculations.

Zinc oxide is an n-type semiconductor [14] in which group III element contamination can cause an increase in electrons in the conducting film. Experiments have revealed that a little quantity of aluminum or gallium (Al or Ga) impurities can contaminate the thin films of zinc oxide. This material will have low electrical resistance (approximately $10^{-4}$ Ω·cm), mobility, and a larger carrier density while preserving sufficient transparency [15]. The optical, electrical, and structural characteristics of zinc oxide films polluted with the element Al were examined in this work due to the relevance of this topic.

**2. Materials and methods**

*2.1. Samples synthesis*

The synthesis of samples was done on two glass and silicon substrates in this study. The first step in starting a sol-gel synthesis process is to choose an acceptable solubilization technique. 0.6 M zinc acetate solution (ZnAC) with methanol solvent and monoethanolamine stabilizer (MEA) with a mass ratio (r = MEA / ZnAC) of 0.6 was utilized in this approach. MEA was progressively added to the zinc acetate solution after it was put in ultrasonic equipment for half an hour. After 24 hours, the final tubercle was clear and sediment-free, and it was ready to be filmed. Immersion at a speed of 5 cm/min and spin at a speed of 3000 rpm/min for 20 seconds were used to synthesize the material. Drying took place at 250°C, followed by annealing at 500°C in an electric oven that was pressured for one hour. The samples in this investigation were dried using the immersion technique at 250°C at a speed of 7 cm/min. This process was performed three times before the films were annealed in an electric oven at air pressure for one hour at 450° C. The cell was constructed using acetate zinc 0.6 M as a precursor and methanol as a solvent. Aluminum impurities were introduced as aluminum nitrate, with atomic percentages distinct from Zn atoms.

*2-2-Methods of analysis and characterization of samples*

*X-ray diffraction spectrum (XRD)*

Useful information on the produced phases and material structure, as well as average crystallite diameters and lattice constants, may be acquired by measuring the X-ray diffraction spectrum [15-15]. The maximum peak width of the spectrum rises with decreasing thickness in crystallite materials. The average size of crystallites may be calculated using XRD spectrum data and Equation (1), often known as the Scherer equation [17-16]:

$$D = \frac{0/9\lambda}{\beta \cos\theta} \quad (1)$$

Where D, λ, θ, and β are the average size of the crystallites, the applied X-ray wavelength, the Bragg angle, and Full Width at Half Maximum (FWHM), respectively. The distance between the crystallite lattice plates (dhkl) can also be computed using Equation (2), often known as the Bragg equation [18]:

$$۲d_{hke} \sin(\theta) = n\lambda \quad (2)$$

Where n is the diffraction order, λ is the X-ray wavelength, θ is the diffraction angle, and dhkl are the distances of the lattice plates, which are denoted by Miller indices (hkl). Bruker axis model B8-advance with Cuk radiation line with a wavelength of 1.5406 A° was used to analyze X-ray diffraction spectra of the materials produced in this work. This device works by measuring the strength of waves traveling through the sample (with subfilm) and subfilm (without subfilm) (control). The transgression spectra of the materials generated in this study were measured using a Shimadzu UV-Vis spectrometer instrument model 1800-UV situated in Shahroud University of Technology's nanophysics laboratory.

**Calculating the absorption coefficient (α) and bandgap (Eg)**

The absorption coefficient () and optical band gap (Eg) can be computed using the trajectory spectrum. When an electromagnetic wave of magnitude I0 is irradiated into a medium with a thickness of d, some of the light transmits through the material, some are reflected, and some is absorbed. If the film's reflectance is insignificant, equation (3) can be used to compute the absorption coefficient. Lambert's empirical connection [55-56] is an example of this. In this equation, α, T, and d represent the absorption coefficient, the amount of material transmittance, and the thickness of the studied film, respectively.

$$I = I_{.} \exp(-\alpha d) \Rightarrow a = \frac{-۱}{d} \ln(T) \quad (3)$$

**Calculating optical constants**

Equations (4) and (5) [19] can be used to compute the refractive index (n) in the transmittance spectrum in the region where it is zero:

$$n_f = \sqrt{N + \sqrt{(N^{۲} - S^{۲})}} \quad (4)$$

$$N = \left(\frac{۲S}{T_m}\right) - \left(\frac{S^{۲} + ۱}{۲}\right) \quad (5)$$

$T_m$ is the maximum transmittance in these equations, and S is the refractive index of the substrate, which is 1.52 for glass [19].

The amount of porosity at the surface of the samples can also be determined by using equation (5) [19] and the absorption coefficient:

$$P = 1 - \left[ \frac{\left(n_f^2 - 1\right)/\left(n_f^2 + 2\right)}{\left(n_s^2 - 1\right)/\left(n_s^2 + 2\right)} \right]$$

(6)

On the other hand, using Equation (6) and the quantity of reflection from the sample surface, the refractive index can be determined in a different approach. In this equation, k represents the extinction coefficient $k = \frac{\alpha\lambda}{4\pi}$, λ is the descending photon wavelength, and α is the absorption coefficient [15].

$$R = \frac{(n-1)^2 + k^2}{(n+1)^2 + k^2}$$

(7)

The thin film refractive index is determined by the following equation concerning the two maximum, and minimum transmittance ranges on the trajectory curve $T_{M(\lambda)}$ and $T_{m(\lambda)}$, respectively, and the value of the subfilm refractive index, according to Sun Paul:

$$n = \sqrt{M + \left(M^2 - n_s^2\right)^{1/2}}$$

(7)

where

$$M = 2n_s \left[ \frac{\left(T_M - T_m\right)}{T_M T_m} \right] + \frac{\left(n_s^2 + 1\right)}{2}$$

(8)

The film thickness is calculated using the refractive index of the film and two neighboring peaks (or minima) as described in the fundamental equation of interfering waves [20]:

$$d = \frac{\lambda_1 \lambda_2}{\left[2\left(\lambda_1 n_2 - \lambda_2 n_1\right)\right]}$$

(9)

where (n2) n1 is the refractive coefficient corresponding to the wavelengths 1λ (2λ).

The thickness can be computed using the following equation [21] in the situation of adjacent maximum and minimum:

$$d = \frac{\lambda_1 \lambda_2}{\left[4\left(\lambda_1 n_2 - \lambda_2 n_1\right)\right]}$$

(10)

If the film's transverse spectrum lacks maximum and minimum points, another method for determining the optical constant of thin films should be adopted. Considering various physical limits for semiconductors and insulators in the dispersion area [22] is one of these strategies provided by Chambouleyron et al.

The thickness of the synthesized films was determined in this work using data from the Puma program and equations (9) and (10) (11). However, because the spectrometer at Shahroud University of Technology's Faculty of Physics can detect the proportion of absorption and reflection, the thickness d may be estimated by measuring A, R, and T using equation (3), visualizing curve A in terms of T, and finding the curve's parameters.

**Measuring the resistivity**

The resistivity can be computed using Equation (12) by the film thickness (d) and regardless of the length and breadth of the sample on which the measurement was taken:

$$\rho = R_s d C_f$$

(12)

$C_f$ is a correction factor in this case [2]. The company's four-device device (Jundel) model (AM3-AR) housed in Shahroud University of Technology's nano-physics laboratory was employed in this study.

The mobility of carriers can also be computed [23] by having resistivity and measuring the Hall coefficient - establishing the effective density of load carriers and their kind - and utilizing a set of equations (13).

$$\begin{cases} \sigma = \dfrac{1}{\rho} \\ \sigma = ne\mu \Rightarrow \mu = \dfrac{\sigma}{ne} \end{cases}$$

(13)

where e, σ, and μ represent the electron charge, conductivity, and mobility of carriers, respectively.

**Hall effect test**

The Hall effect is the most popular method for measuring carrier density directly. Due to the deflection of moving charges in their path (due to the presence of a magnetic field), a driving force occurs across the sample and perpendicular to the magnetic field when an electric current transmits through a semiconductor in a magnetic field so that the magnetic field is perpendicular to the current transmittance through it [2].

We have the following equation for electrons moving at $v_x$ in a magnetic field $B_z$:

(14)

$$\begin{cases} e\varepsilon_y = ev_x B_z = j_x B_z / n \\ R_H = ZV_H / I_x B_z = 1/ne \end{cases}$$

Where $j_x=nev_x$, $I_x$, $V_H$, and Z are the current density, the current that transmits through the sample, the measured value of Hall voltage, and the sample thickness in the direction of the magnetic field, respectively. Accordingly, $R_H$ needs to depend on the *e*-sign.

**3. Results and discussion**

*3.1. X-ray diffraction spectrum*

Figure 1 illustrates a simultaneous measurement of an X-ray diffraction spectrum of impurity-free samples and samples polluted by Al impurities. Three peaks owing to diffraction from plates (100), (002), and (101) are visible in this spectrum, all of which are connected to the creation of the hexagonal structure of zinc oxide. As shown, peak intensity (002) fell considerably as sample contamination increased, while differences in peak intensities (100) and (101) between contaminated and uncontaminated samples were minor. Furthermore, as the proportion of aluminum was increased, the intensity of the above peaks did not vary much (less than 10 percent). Peak widening (002) might be related to stress caused by the radius difference between zinc and aluminum ions [24].

Aluminum is a divalent element that belongs to the periodic table's third group (trivalent). As a result, by introducing Al impurities into the zinc oxide structure, Al atoms might potentially replace Zn atoms in the crystallite lattice. Because Al [25] atoms have a lower radius (approximately 1.25 °A) than Zn [about 88], this might impact crystallite lattice constants (about 1.34 °A). The breadth of the peaks and, as a result, the structural quality of the samples have been impacted as the degree of contamination has increased.

The tissue coefficient for the samples was determined to assess the growth direction. Table 1 shows the outcomes of these computations (1). These findings suggest that the [002] direction is the favored development direction in all samples.

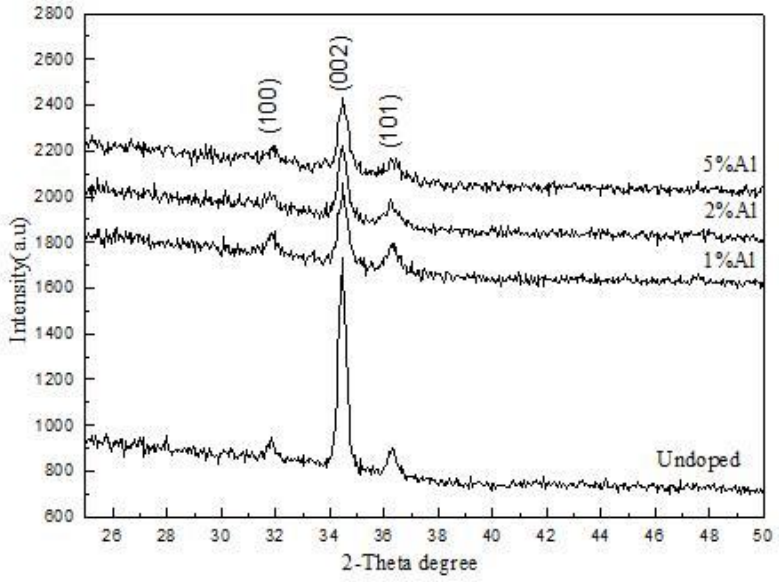


**Figure 1.** X-ray diffraction spectra of contaminated samples with different atomic percentages of Al

**Table 1.** TC coefficients and I / I0 ratios for non-contaminated and Al contaminated samples

| %5 Al | | % 2Al | | %1 Al | | Non-contaminated | | Diffraction of plates |
|---|---|---|---|---|---|---|---|---|
| TC | $(I/I_0)$ | TC | $(I/I_0)$ | TC | $(I/I_0)$ | TC | $(I/I_0)$ | |
| 0.484 | 26.3 | 0.444 | 23.52 | 0.577 | 31.25 | 0.290 | 12.5 | (100) |
| 1.839 | 100 | 1.889 | 100 | 1.846 | 100 | 2.324 | 100 | (002) |
| 0.675 | 36.8 | 0.666 | 35.29 | 0.577 | 31.25 | 0.386 | 16.6 | (101) |

Equations (1) and (3) were used to compute crystallite size and lattice parameters, with the results shown in Table (2). These findings reveal that when impurity increases, the network's c-parameter remains almost constant (about 5.2027 angstroms), which is consistent with normal card values (5.20661 angstroms). The rate of change of the network

parameter is more than the recorded value of standard cards (3.24982 Angstrom), which are mostly compatible with each other, for example, with 2% aluminum alloy. In addition, when the impurity percentage increased, the crystallite diameters shrank. Indeed, contaminants may lower the germination threshold radius and allow the growing process to continue. Numerous studies [27-26] have shown similar outcomes.

**Table 2.** Bandgap values and grain size and lattice parameters in impregnated films with Al.

| Percentage of Al contamination | Dimensions of crystallites (nm) | θ2 Plate angle (002) | ( d)$A^0$ (002) | Network parameter c (A0) (002) | Percentage deviation (002) d compared to standard cards | ( d)$A^0$ (100) | Percentage deviation (100) d compared to standard cards | Network parameter a (A0) (100) |
|---|---|---|---|---|---|---|---|---|
| Non-contaminated | 50 | 34.45 | 2.6013 | 5.2027 | 0.07 | 2.8071 | 0.26 | 3.2422 |
| 1% atomic | 40 | 34.50 | 2.5969 | 5.1939 | 0.24 | 2.7908 | 0.85 | 3.2234 |
| 2% atomic | 45 | 34.45 | 2.6013 | 5.2072 | 0.07 | 2.8113 | 0.11 | 3.2469 |
| 5% atomic | 38 | 34.50 | 2.5969 | 5.1939 | 0.24 | 2.8030 | 0.40 | 3.2375 |

### 3.2. Studying the optical properties

Figure 2-a depicts the sample trajectory spectrum. As can be observed in this diagram, the average sample transmittance without contamination in the area of the measured wavelength is about 80%, and after contamination is around 60%. As shown, the flow of samples reduced as contaminants were introduced. The transmittance percentage similarly increases with rising pollution to 1%, then decreases (by around 20%) before increasing again with increasing pollution to 2%. A declining trend in the percentage of transmittance is noticed, with a further increase in the percentage of contamination to around 5%. Aluminum atoms that are not situated at Zn sites can behave as scattering centers. As a result, increasing the proportion of aluminum can justify the loss in permeability. These findings are consistent with the findings of group R. M. Mehra [27]. In addition, when the size of the crystallite diminishes, the dispersion across the grain boundaries may grow, reducing the transmittance.

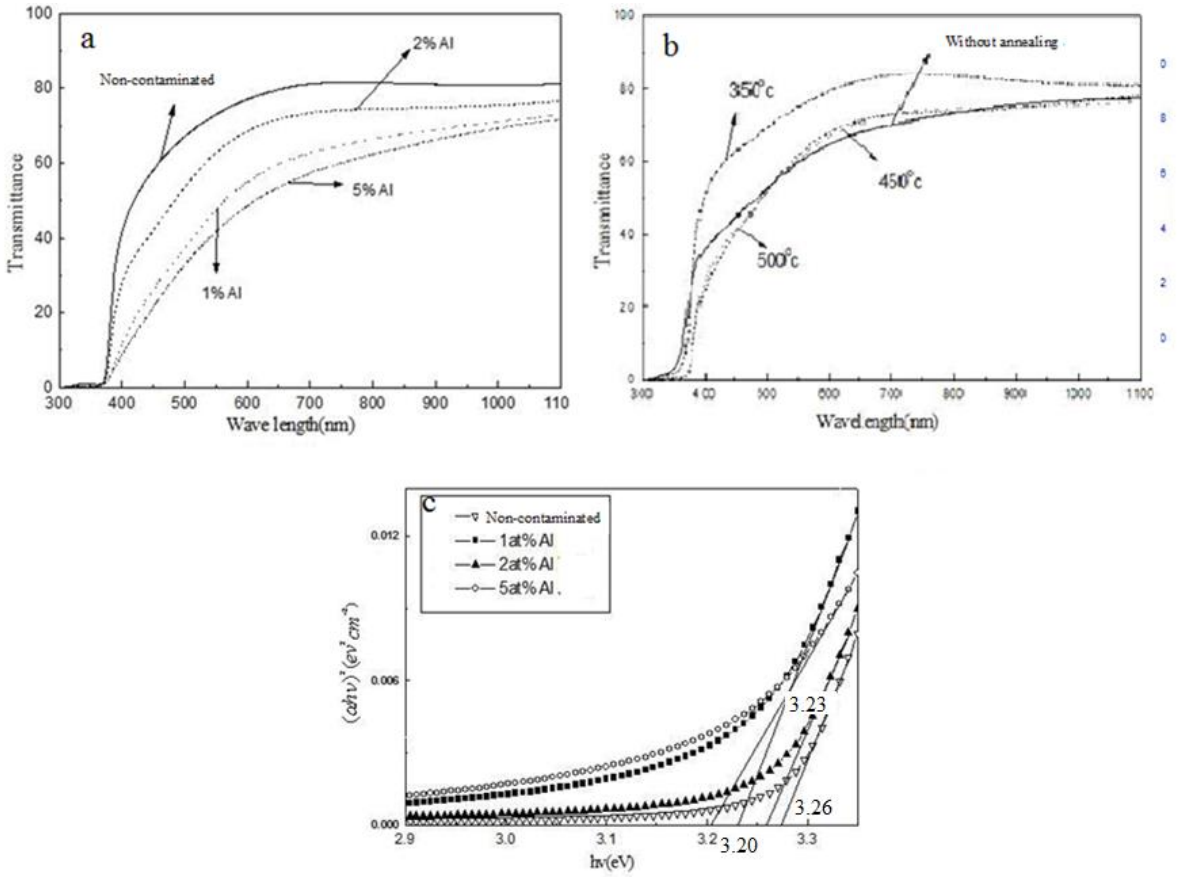


**Figure 2.** a ) Transaction spectra of samples without contamination and Al contamination. b) The transverse spectra of the sample were contaminated with Al 2% at different annealing temperatures.,
c) The changes of $(\nu h\alpha)^2$ in terms of the energy of the incident photon at different pollution percentages Al, Bandgap changes in contaminated and non-contaminated samples.

.

Contamination of samples with Al, on the other hand, may enhance the surface roughness of the films or cause porosity on their surface [28]. As a result, the increase in permeability in the sample contaminated with 2% aluminum might be attributed to an increase in porosity in the sample's surface, which lowers surface dispersion and hence increases permeability.

We can get a more accurate characterization of this sample by looking at the trajectory spectrum for samples with 2% aluminum contamination that have been annealed at 350, 450, and 500 degrees. The figure shows the results of this research (2-b). The percentage of transmittance in the sample annealed at 350 ° C is higher than in all other samples. However, the absorption edge has migrated to longer wavelengths in all annealed samples.

As illustrated, adsorption begins in the 370 nm wavelength region on non-contaminated materials and moves somewhat towards lower energies as the number of impurities rises. The absorption coefficient (α) may be calculated from the data of

the samples' absorption spectra, and the graph of changes $^2$ (vh) can be plotted in terms of the photon energy acquired from Equation (4), and the bandgap computed from there (Figure 2-c).

summarizes the findings (3). As the bandgap figures reveal, the bandgap narrowed as the samples became more contaminated. For a sample with 5% pollution, the amount of change is around 50 meV. This decrease might be due to the

particle impact itself. The presence of Al in the bandgap (below the conduction band) may have caused impurity levels to rise, displacing the adsorbed edge.

### 3.3. Surfaces morphology

Scanning electron microscopy pictures can provide more precise information about the structure as well as the surfaces of the generated objects. The presence of a Y-shaped band pattern in the structure of all samples is shown by the accuracy of the recorded images (without contamination and contaminated). The banding pattern of pure samples with 2% contamination, on the other hand, is more comparable to each other. Furthermore, the tape patterns of the samples with 1% and 5% contamination are more comparable to one another. The diameter of the bands grows with the contamination of the materials, as shown in these images (from roughly 300 to 600 nm). However, with a 5% increase in pollution, the diameter of the strips seemed to have shrunk once again(fig.3).

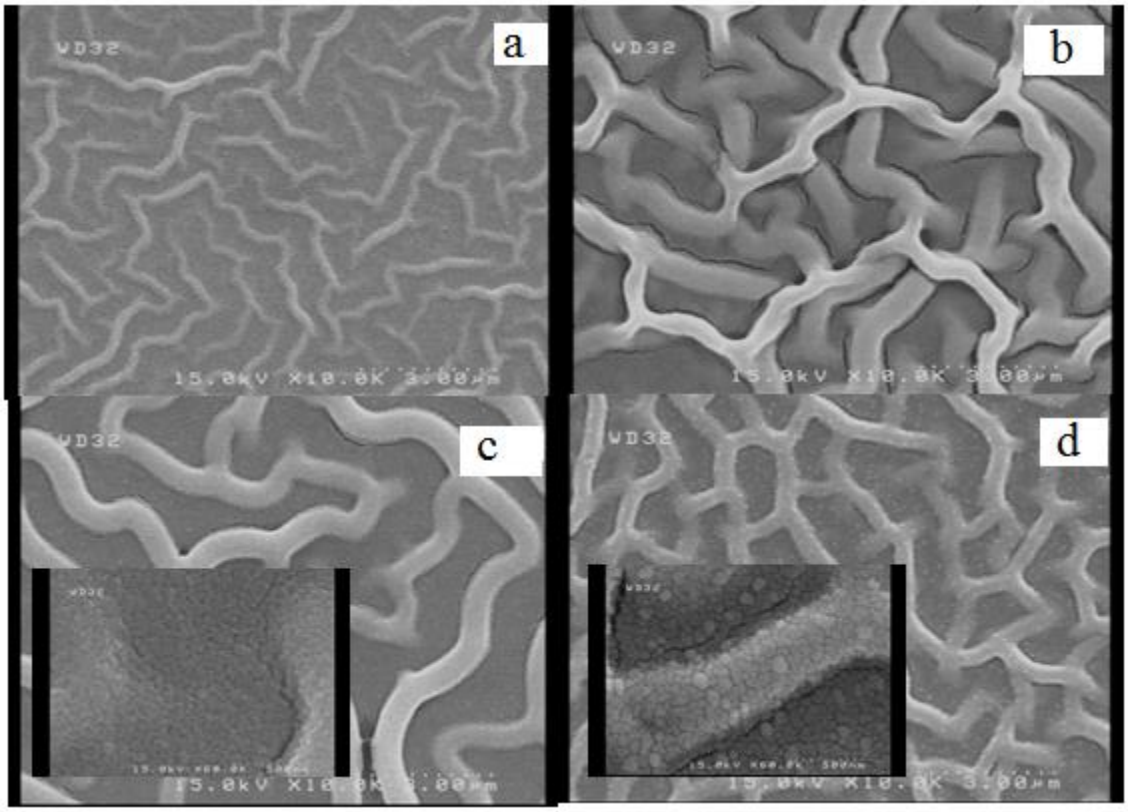


**Figure 3.** FESEM image of thin films of zinc oxide impregnated with different percentages of impurities Al a) without impurities b) 1% atomic c) 2% atomic d) 5% atomic.

With a 5% aluminum impurity, for example, virtually white particles with an average width of 100 nm may be observed distributed across the measurement range in the images captured in Figure 3. This might imply the creation of new phases, which would need further measurements such as EDAX to study further. The Y group created this style of grain pattern on the surface. Caglar et al. have also been found to indium contamination of thin films of zinc oxide [29]. A similar structure may be found in another work by U. N. Miti. However, this group has explored the effect of manganese contamination on zinc oxide thin films [30].

### 3.4. Studying the electrical properties

The electrical resistance of produced zinc oxide films was evaluated using a four-legged apparatus to explore their electrical characteristics. Figure (4) depicts the variations in specific strength of contaminated films with various Al atomic percentages. The resistivity drops with a modest percentage of Al impurity (atomic order size), decreases to a minimum with a rise of up to 2%, and then increases with a further increase in impurity, as expected. The increase in charge carriers owing to the presence of Al impurities is thought to be the cause of the decrease in resistivity with aluminum contamination. However, increasing the number of impurity atoms causes these atoms to behave as scattering centers, increasing the film's surface strength. Such results are in line with the report by D. C. Cameron that studied the effect of pollution percentage and annealing temperature in different environments. However, the resistance reported by this group is of lower levels [31].

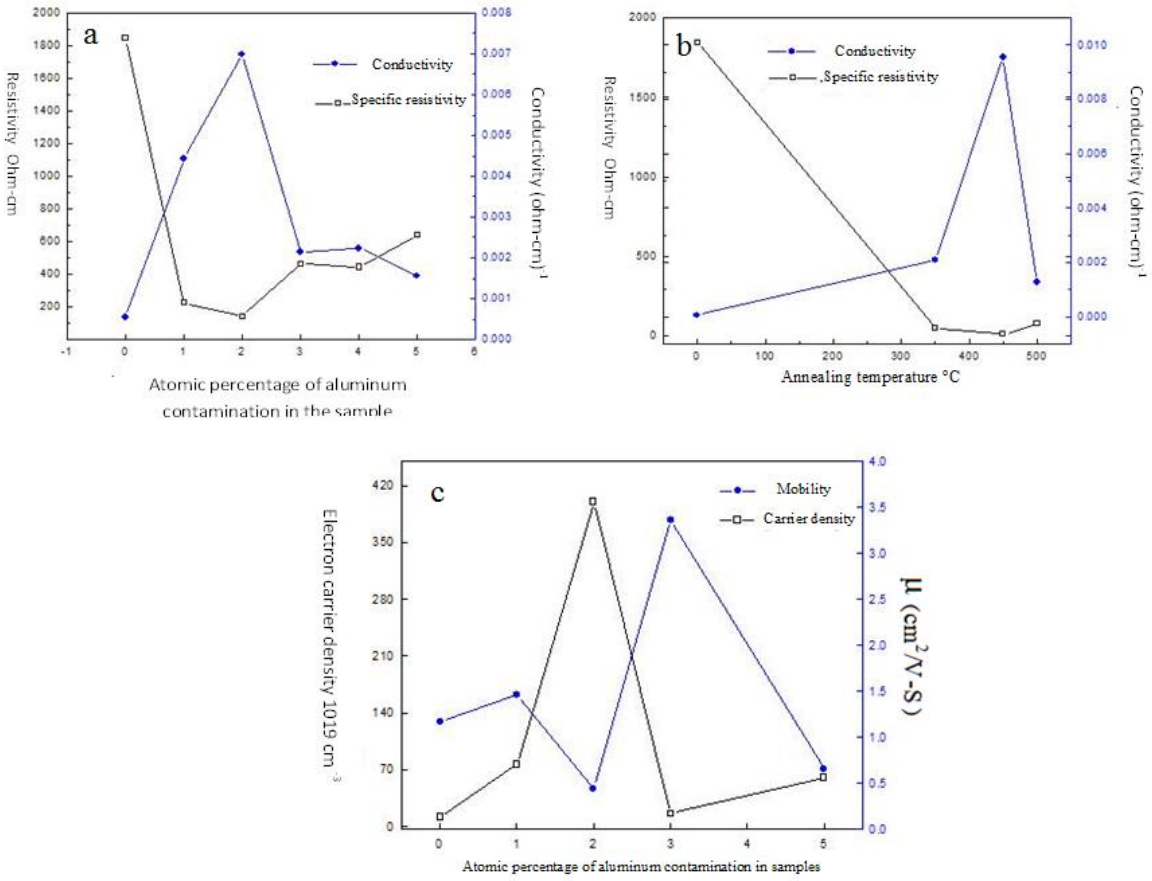


**Figure 4.**a , b) Changes in resistivity and conductivity by entering the impurity percentage of Al and annealing temperature. c) Changes in carrier mobility and density by changing the percentage of impurities Al.

The resistivity and conductivity for films with 2% aluminum contamination were tested at three annealing temperatures of 350, 450, and 500 ° C, as well as without annealing, to explore the influence of annealing temperature on the process of lowering surface resistance. These variations reveal that the samples had the lowest specific strength and the maximum conductivity at the annealing temperature of 450 ° C. (Figure 4).

Calculating the conductivity and density of carriers for the samples reveals that these values have the maximum value for a 2 percent aluminum impurity percentage and that this value declines as the number of impurities increases. In addition, this sample's carrier mobility is the lowest, which is consistent with the study conducted by Kim et al. [32].

**4. Conclusion**

Thin films of zinc oxide tainted with aluminum were produced in this investigation. The X-ray diffraction spectrum of these samples comprises three peaks owing to diffraction from plates (100), (002), and (101) associated with the creation of a hexagonal structure of zinc oxide, according to the results of characterization. Sample contamination reduces peak intensity (002) substantially. The strength of peaks (100) and (101) in infected and uncontaminated samples differs just a little. Furthermore, as the proportion of aluminum is increased, the intensity of the above peaks does not alter much (less than 10 percent). Peak widening (002) might be related to stress caused by the radius difference between zinc and aluminum ions. The polluted films' electrical characteristics were also tested. These results revealed that the resistivity of the synthesized films drops by a small amount of impurity to a significant order, resulting in a sample with a minimum impurity of roughly 2% and increasing again with the addition of further impurities. The sample has a maximum impurity percentage of 2%, according to the conductivity and density of carriers calculated for all samples, which lowers as the amount of contaminants

increases. The average passing of the sample without impurities is around 80%, which is lowered to about 60% by the introduction of contaminants, according to measurements of the transgression spectra of the samples. Furthermore, the adsorption edge of impurity-free samples is in the 370 nm wavelength region, which moves to lower energies as the number of impurities rises. The morphology of the surfaces was examined using FESEM images, which revealed that the crystal pattern is in the form of Y-shaped branches with a diameter of approximately 500 nm. Only the diameter and length of the branches alter as a result of pollution, as shown in these photographs.

**Acknowledgement**

We appreciatively acknowledge monetarily and support from the Shahroud University of Technology.

**Source of Funding**

*This work was supported by* Shahroud University of Technology.

**Conflict of Interest**

The author declares that she has no known competing financial interests or personal relationships that could have appeared to influence the work reported in this paper.

## References

1. Dean Campbell, 2005, *The journey of the nanoworld using logo parts*, translated by Farima Agand and Nader Naderi, first edition, Ayeh Publishing Institute, Tehran.

2. H. M. Rosenberg, *Solid State Physics*, translated by Dr. Hossein Eshghi and Dr. Hassan Azizi, 1997, University Publishing Center, First Edition, Tehran.

3. E. Burestein, Phy. Rev., 93 (1954) 632.

4. G. B. Palmer , K. R. Poeppelmeier, T. O. Mason, Chem. Mater. 1997, 9, 3121-3126.

5. Hadi Savalani, 2005, *Fundamentals of Surface Science in Nanotechnology*, Volumes I and II, First Edition, Institute of Publishing and Printing, University of Tehran, Tehran.

6. E. Guziewicz,,M. Godlewski, T. Krajewski and et al. , Journal of Applied Physics 105 (2009) 122413.

7. T. Ehara, T. Ueno, J. Abe, Phys. Status Solidi A 207 (2010) 1600–1603.

8. J. Lee, Z. Li, M. Hodgson, J. Metson, A. Asadov, W. Gao, Current Applied Physics 4 (2004) 398–401.

9. M. Guo, C.Y. Yang, M. Zhang , Y. J. Zhang , T. Ma , X. Wang, X. D. Wang, Electrochimica Acta 53 (2008) 4633–4641.

10. J. M. Khoshman, M. E. Kordesch, Thin Solid Films 515 (2007) 7393–7399.

11. W.J. Fan, X. B.Xia & et al., Journal of Applied Physics, 99 (2006) 013702.

12. A. K. Zak, M. E. Abrishami, W.H. Abd. Majid, R. Yousefi, S.M. Hosseini, Ceramics International 37 (2010) 393-398.

13. S. Rani, P. Suri, P. K. Shishodia, R. M. Mehra, Solar Energy Materials & Solar Cells 92 (2008) 1639–1645.

14. N. J. Awang, M. Aziz and A. R. M. Yusoff, Solid State Science and Technology, 16 (2008) 45-54.

15. M. Caglar, S. Ilican, Y. Caglar, F. Yakuphanoglu, Applied Surface Science 255 (2009) 4491–4496.

16. M. Mohammadi, M. R. Rokn-Abadi, H. Arabshahi, Indian Journal of Science and Technology, 3 (2010) 110-112.

17. S. Suwanboon1, R. Tanattha, R. Tanakorn, Songklanakarin J. Sci. Technol. 30 (1) (2008), 65-69.

18. Ashcroft, Neil W., Solid state physics, 1976 saunders college publishing.

19. M. Dutta, S. Mridha, D. Basak, Applied Surface Science 254 (2008) 2743–2747.

20. V. Pandey, S. K. Tripathi, A. Kumar, Journal of Ovonic Research, 3 (2007) 29-38.

21. Ludmila Ekratova, translated by Dr. Hadi Savalani, *Physics of Thin Films and Surfaces*, University Publishing Center, First Edition, 2006.

22. I. Chambouleyron, J. M. Martínez, A. C. Moretti, and M. Mulato, Appl. *Optics* ,36 (1997) 8238.

23. S. M. Z, *Physics and technology of semiconductor components*, translated by Gholam Hossein Sadir Abedi, 1985, first edition, Imam Reza University, Mashhad.

24. H. M. Zhou, D. Q. Yi, Z. M. Yu, L. R. Xino, J. Li, *Thin solid film*, 515 (2007) 6909.

25. Http://fa.Wikipedia.org

26. B. Gupta, A. Jain, R. M. Mehra, J. Mater. *Sci. Technol*., 26(3) (2010) 223-227.

27. S. Ilican, Y. Caglar, M. Caglar, F. Yakuphanoglu, J. Cui, Physica E 41 (2008) 96–100.

28. S. P. Shrestha, R. Ghimire, J. J. Nakarmi & et al., Bull. Korean Chem. Soc., 31 (2010) 112-115.

29. Li-Yu Lin, Dae-Eun Kim, *Thin Solid Films* 517 (2009) 1690–1700.

30. U. N. Maiti, P. K. Ghosh, S. Nandy, K. K. Chattopadhyay, Physica B 387 (2007) 103–108.

31. M. J. Alam, D. C. Cameron, *Second International Conference on Electrical and Computer Engineering* ICECE 2002, 26-28 December 2002, Dhaka, Bangladesh, pages 246-249.

32. S. P. Shrestha, R. Ghimire, J. J. Nakarmi & et al., Bull. Korean Chem. Soc., 31 (2010) 112-115.